On seasonal signals in geodetic time series

James L. Davis,[1] Brian P. Wernicke,[2] and Mark E. Tamisiea[3]

[1] We explore implications for modeling and noise analysis of stochastic seasonal processes of climatic origin in geodetic time series. Seasonal signals are generally modeled as sinusoids with annual periods (and harmonics thereof), each with constant amplitude and phase. However, environmental noise that underlies the seasonal signal in geodetic time series has a reddened power spectral density (PSD). We investigate the form of the PSD of a time series having a stochastic seasonal component and find that for frequencies greater than the nominal seasonal frequency, the PSD of the time series reflects the PSD of the seasonal amplitudes. For example, if the PSD of the seasonal amplitudes can be expressed as an inverse power law, then the PSD of the time series will behave as an inverse power law for high frequencies. Stochastic seasonal variability will also induce a peak near the nominal seasonal frequency in addition to that of the mean seasonal signal and will be relatively flat below this frequency. It is therefore possible that some of the noise in Global Navigation Satellite Systems (GNSS) time series reported by others may be associated with neglecting the stochastic component of the seasonal signal. We use a GNSS time series from site ZIMM as an example to demonstrate the existence of a variable seasonal signal (without attributing its cause), and we use an example Gravity Recovery and Climate Experiment (GRACE) time series from Alaska to demonstrate that use of a nonstochastic seasonal model can have a significant impact on the value and uncertainty of time-variable rates estimated from the time series.

1. Introduction

[2] The study of noise in geodetic time series has been pursued for a number of important reasons. Understanding noise in the time series is vital for the detection and interpretation of the signals of interest. It is especially important in understanding the uncertainties of parameters estimated from the time series [e.g., *Langbein and Johnson*, 1997; *Zhang et al.*, 1997; *Beavan*, 2005; *Langbein*, 2008; *Santamaría-Gómez et al.*, 2011]. Noise can also reveal shortcomings in the models and techniques used for the underlying analysis from which the time series are obtained [e.g., *Penna and Stewart*, 2003; *Penna et al.*, 2007; *King et al.*, 2008; *King and Watson*, 2010].

[3] The "noise" in the time series is defined to be the residual signal relative to a model that is estimated prior to or simultaneous with the noise analysis. This model generally includes a seasonal signal, for seasonal signals are present in a variety of geodetic time series. In some cases, the seasonal

signals reflect geophysical signal. For example, some Global Navigation Satellite Systems (GNSS) sites experience a real seasonal motion associated with local environmental effects, such as rain [e.g., *King et al.*, 2007], temperature [e.g., *Prawirodirdjo et al.*, 2006], surface loading [e.g., *van Dam et al.*, 2001], and aquifer pumping [e.g., *Bell et al.*, 2002]. Other environmental effects do not involve actual motion of the antenna phase center. For example, multipath/ scattering [e.g., *Elósegui et al.*, 1995] is not modeled in the phase solutions and thereby induces a systematic error in the position estimate that appears as correlated noise in the time series [e.g., *Park et al.*, 2004; *King and Watson*, 2010].

[4] The seasonal signal is typically represented by sums of sinusoids with annual frequency and its harmonics. Whether this seasonal signal represents systematic error (the elimination of which by the development of improved models is always preferable) or true climatic signal, it is important to model this seasonal signal since it can impact parameters of interest estimated from the time series, particularly the site velocity [e.g., *Blewitt and Lavallée*, 2002; *Bos et al.*, 2010]. However, there is reason to expect that the seasonal signal in geodetic time series (itself being a response to environmental changes) is not time-invariant. Environmental variables are known to have a red power spectrum and are typically expressed in terms of an inverse power law [e.g., *Vasseur and Yodzis*, 2004]. Biological populations, for example, are known to exhibit a red spectrum in response to environmental

---

[1]Lamont-Doherty Earth Observatory, Columbia University, Palisades, New York, USA.
[2]Division of Geological and Planetary Sciences, California Institute of Technology, Pasadena, California, USA.
[3]National Oceanography Centre, Liverpool, UK.

noise that underlies seasonal variability [e.g., *Halley and Inchausti*, 2004].

[5] Several previous analyses have taken interseasonal variability into account. *Murray and Segall* [2005] modeled the seasonal amplitudes as a random walk process and used a Kalman filter to estimate the time-dependent parameters, an approach used in the study of *Wernicke and Davis* [2010] as well as here. *Davis et al.* [2006] used piecewise continuous linear polynomials to represent the seasonal amplitudes, and *Bennett* [2008] employed a more general representer method.

[6] Recent studies have identified periodic noise in GPS time series at harmonics of the GPS draconitic frequency [e.g., *Barrett*, 2008; *Ray et al.*, 2008; *Tregoning and Watson*, 2009; *King and Watson*, 2010]. The draconitic period for the GPS constellation is ∼351.4 days [*Tregoning and Watson*, 2009], making the draconitic frequency ∼1.04 cycles per year (cpy). Thus, an individual time series would have to have a length of ∼25 years to separate noise at the fundamental draconitic frequency and the climatic seasonal frequency of 1 cpy. Noise in the draconitic spectrum is therefore identified by stacking power spectra of GPS time series. Near the lower harmonics (annual and semiannual), climatic seasonal signals appear to dominate the error spectrum [*Barrett*, 2008; *Ray et al.*, 2008], although both unmodeled multipath [*King and Watson*, 2010] and atmospheric loading contributions at tidal periods [*Tregoning and Watson*, 2009] have been shown to yield noise at the draconitic annual and semiannual frequency. In this study we assume that the term "seasonal" applies to climatic seasonal signals, and we leave to future study the problem of separation of climatic and draconitic signals.

[7] Below, we explore the implications for modeling and noise analysis of stochastic seasonal processes of climatic origin in geodetic time series. We investigate the form of the power spectral density of a time series having a stochastic seasonal component. We then model this seasonal variability using a Kalman filter in two types of geodetic time series. The first is a time series of the vertical coordinate of site position of a GNSS site. We also consider a time series of surface mass calculated from Gravity Recovery and Climate Experiment (GRACE) data, wherein the observed seasonal signal is greater than the variability in the rate. We begin by developing a theory for expressing this variability, focusing on the annual signal.

2. Theory

[8] In this section we develop an expression for the time-variant seasonal process as the sum of a deterministic component with an annual period (which we term the "annual signal") and a zero-mean stochastic component. The sum of these two components creates a harmonic process with a variable period centered on 1 year; we use the term "stochastic seasonal process" for this combined process. Higher-order harmonics (semiannual and higher) are also involved in the description of seasonal processes. We ignore these higher harmonics in the development in this section, but the expressions can be applied to all of the harmonic components.

[9] To develop an expression for the power spectral density (PSD) of the stochastic seasonal process, it is simplest to adopt the following generalization of the standard time-invariant annual process [e.g., *Young et al.*, 1991; *Durbin and Koopman*, 2001]:

$$x(t) = a_1(t)\cos 2\pi f_\circ t + a_2(t)\sin 2\pi f_\circ t, \quad (1)$$

where $f_\circ = 1$ cpy and $a_1(t)$ and $a_2(t)$ are instantaneous time-variable amplitudes. Equation (1) can of course be written in the equivalent form

$$x(t) = A(t)\cos \theta(t) = A(t)\cos[2\pi f_\circ t + \phi(t)], \quad (2)$$

where $\theta(t)$ is the total instantaneous phase, $A(t)$ is the instantaneous amplitude, and $\phi(t)$ is the instantaneous phase offset. The phase offsets and amplitudes in equations (1) and (2) are related by

$$A^2 = a_1^2 + a_2^2 \quad \text{and} \quad \phi = -\tan^{-1}\left(\frac{a_2}{a_1}\right). \quad (3)$$

As discussed above, we develop only the annual terms of the stochastic seasonal signal.

[10] The motivation for equations (1) and (2) lies in the observation that any small segment of the time series may be described as a nearly annual sinusoid, assuming that the amplitude does not change too rapidly over the period $f_\circ^{-1}$. Equation (2) implies that the instantaneous frequency f varies as a function of time through the variation of ϕ as

$$f(t) = \frac{1}{2\pi}\frac{d\theta(t)}{dt} = f_\circ + \frac{1}{2\pi}\frac{d\phi(t)}{dt}, \quad (4)$$

and we therefore find no need explicitly to include a time dependence for $f_\circ$ in equations (1) or (2).

[11] In equation (1), we take $a_1(t)$ and $a_2(t)$ to be stochastic processes. Without any loss of generalization, we can decompose each of these into the sum of a long-term mean and a zero-mean stochastic component:

$$a_i(t) = \bar{a}_i + \delta a_i(t) \quad i = 1, 2. \quad (5)$$

We would like for simplicity to be able to assert that the stochastic processes $\delta a_1(t)$ and $\delta a_2(t)$ are independent, but we have no evidence for this. The sinusoidal amplitude $A(t)$ in equation (2) may vary significantly in terms of its mean, but we do not expect the phase offset $\phi(t)$ to vary too rapidly or significantly, since this would not yield a coherent recognizable seasonal signal. If the phase offset $\phi(t)$ is the constant value $\phi_\circ$, then from equations (3) and (5),
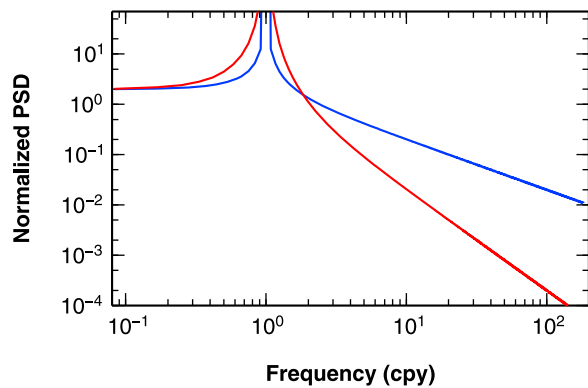
$$\bar{a}_2 + \delta a_2(t) = -[\bar{a}_1 + \delta a_1(t)]\tan \phi_\circ. \quad (6)$$

Thus, in the case of constant phase offset the two stochastic processes $\delta a_1(t)$ and $\delta a_2(t)$ are linearly dependent on one another. Taking the expectation of both sides in equation (6), we find that

$$\tan \phi_\circ = -\frac{\bar{a}_2}{\bar{a}_1}. \quad (7)$$

[12] To express a temporal variation in the phase offset, we introduce an additional zero-mean stochastic process $\delta b(t)$ such that

$$\bar{a}_2 + \delta a_2(t) = \frac{\bar{a}_2}{\bar{a}_1}[\bar{a}_1 + \delta a_1(t)] + \delta b(t). \quad (8)$$

Figure 1. Normalized PSD of equation (15) for $\alpha = 1$ (blue) and $\alpha = 2$ (red). Only positive frequencies are shown; the PSDs are symmetric about $f = 0$.

Substituting this expression into equation (1) yields

$$x(t) = \left[1 + \frac{\delta a_1(t)}{\bar{a}_1}\right](\bar{a}_1 \cos 2\pi f_\circ t + \bar{a}_2 \sin 2\pi f_\circ t) + \delta b(t) \sin 2\pi f_\circ t. \quad (9)$$

The first term on the right-hand side of equation (9) expresses the time-variable, fixed phase offset part of the seasonal signal, whereas the second term enables the phase offset ϕ to vary with time.

[13] Equation (9) also enables us to decompose $x(t)$ into a purely annual sinusoidal term $\bar{x}(t)$ and a zero-mean stochastic seasonal process $\delta x(t)$:

$$x(t) = \bar{x}(t) + \delta x(t), \quad (10)$$

$$\bar{x}(t) = \bar{a}_1 \cos 2\pi f_\circ t + \bar{a}_2 \sin 2\pi f_\circ t, \quad (11)$$

$$\delta x(t) = \frac{\delta a_1(t)}{\bar{a}_1}(\bar{a}_1 \cos 2\pi f_\circ t + \bar{a}_2 \sin 2\pi f_\circ t) + \delta b(t) \sin 2\pi f_\circ t. \quad (12)$$

In equation (11), the bar over x indicates an ensemble average. The temporal variability of $\bar{x}(t)$ arises solely through the annual sinusoidal terms.

3. PSD of Seasonal Signals

[14] As discussed in section 1, the PSD is often used in analysis of GNSS time series to assess noise. In this section, we explore the implications for the PSD of stochastic seasonal processes.

[15] Using equation (12), we can find an expression for the PSD of the stochastic seasonal process. We assume that the stochastic processes δa_1 and δb have power spectral densities $S_{a_1}(f)$ and $S_b(f)$, respectively. We further assume that $\delta a_1(t)$ and $\delta b(t)$ are statistically independent. This assumption enables us to neglect cross-power components. The error in this assumption is small as long as the seasonal process maintains a nearly constant phase offset, a reasonable assumption for climate-driven seasonal variations. (*Bennett* [2008], for example, assumed that this phase offset

was constant.) The PSD $S_x(f)$ of the stochastic seasonal process is then given by

$$2S_x(f) = S_a(f - f_\circ) + S_a(f + f_\circ) + S_b(f - f_\circ) + S_b(f + f_\circ), \quad (13)$$

where

$$S_a(f) = \left(\frac{\bar{a}_1^2 + \bar{a}_2^2}{\bar{a}_1^2}\right) S_{a_1}(f). \quad (14)$$

[16] The frequency shifts in equation (13) originate in the sinusoidal multipliers in equation (12) and arise from the so-called modulation theorem of Fourier transforms [e.g., *Bracewell*, 1978]. This modulation has significant implications if $S_a(f)$ and $S_b(f)$ are reddish, which seems likely (see below). For example, the inverse power law form $S(f) = C^2(f_\circ/|f|)^\alpha$, with $\alpha > 0$ and $C^2 = S(f_\circ)$ has been used to describe noise in GPS time series [e.g., *Langbein and Johnson*, 1997; *Zhang et al.*, 1997; *Williams et al.*, 2004; *Beavan*, 2005; *Langbein*, 2008; *Bos et al.*, 2010; *Santamaría-Gómez et al.*, 2011]. (It is common to omit the absolute value signs when considering a one-sided spectrum, but the modulations require that we consider the negative f side as well.) If both $S_a(f)$ and $S_b(f)$ have this form, then

$$S_x(f) = \frac{1}{2}\left(C_a^2 + C_b^2\right) f_\circ^\alpha \left[\frac{|f + f_\circ|^\alpha + |f - f_\circ|^\alpha}{|f^2 - f_\circ^2|^\alpha}\right]. \quad (15)$$

[17] Figure 1 shows the PSD in equation (15) for $\alpha = 1$ (flicker noise) and $\alpha = 2$ (random walk). Figure 1 illustrates some of the important features of stochastic seasonal PSDs. Although the PSDs of the underlying stochastic processes (δa_1, δa_2, and δb) have no spectral lines, the PSD of the stochastic seasonal process has a spectral line at the annual frequency (and harmonics if they are considered). For $|f| \gg f_\circ$, the PSD of the seasonal signal approaches the PSD of the underlying stochastic processes. Thus, for example, for frequencies greater than about 2 cpy, the seasonal signal itself will behave like a random walk (if the underlying stochastic processes are random walks). Another significant feature is that the PSD of the seasonal stochastic process rolls over and is nearly flat for low frequencies.

[18] Another PSD that has been evaluated for describing noise in geodetic time series is the first-order Gauss-Markov (FOGM) process [*Langbein and Johnson*, 1997; *Beavan*, 2005; *Langbein*, 2008; *Santamaría-Gómez et al.*, 2011], which has a PSD given by

$$S(f) = \sigma^2 \frac{\beta}{(2\pi f)^2 + \beta^2}. \quad (16)$$

In an FOGM process, the covariance $R(\tau)$ between two values separated by time τ is $R(\tau) = \sigma^2 \exp(-\beta|\tau|)$. The parameter β is therefore an inverse decay time; *Santamaría-Gómez et al.* [2011] give a median value for β^{-1} of 5.5 months for their geodetic time series. The resulting stochastic seasonal PSD is shown in Figure 2, along with the PSD of the underlying FOGM processes. The stochastic seasonal PSD has features similar to those in Figure 1, including the inverse power law behavior for large f, a resonance (although not
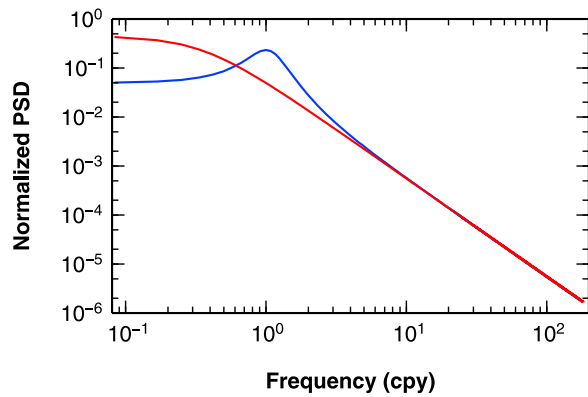
Figure 2. Normalized PSD for the stochastic seasonal process for an FOGM process with β^{-1} = 5.5 months (blue). The underlying FOGM process PSD is shown in red. Only positive frequencies are shown.

nearly as strong) at $f = f_\circ$, and a turnover to a flat spectrum at small f.

4. Examples Using GNSS and GRACE Time Series

[19] Sinusoids of constant annual frequencies (and harmonics, generally just the semiannual period) are typically used for modeling the seasonal variability in geodetic time series. The wide resonance peaks in Figures 1 and 2, however, indicate that a consideration of these pure sinusoidal terms will not remove all the seasonal variability. This situation is illustrated in Figure 3. Figure 3a shows a time series of vertical site position, relative to a reference position, obtained from an analysis of GPS data from site ZIMM by the Scripps Orbit and Permanent Array Center (SOPAC). (See http://sopac.ucsd.edu for a description of data analysis and estimation of offsets for antenna changes.) This particular time series was selected since the site has a long history. The vertical coordinate was used since it often yields a large seasonal signature due to the sensitivity to seasonal vertical motion driven by rain [e.g., *King et al.*, 2007] and temperature [e.g., *Prawirodirdjo et al.*, 2006]. Estimates of the vertical coordinate also have greater sensitivity than do horizontal coordinate estimates to errors associated with elevation-angle-dependent errors such as multipath [e.g., *Elósegui et al.*, 1995] and atmospheric propagation [e.g., *Davis et al.*, 1985; *Herring*, 1986]. We first limit the time series to the final 16 years, a period during which the GPS constellation has been more completely populated. We then edit the data by iteratively fitting the standard model (i.e., straight line plus annual and semiannual sinusoids of constant amplitude) to the data and removing any outlier having a residual with magnitude greater than or equal to four times the weighted root-mean-square (WRMS) postfit residual. Three editing iterations removed ∼3% of the data and reduced the normalized χ^2 statistic by ∼22%. The log file for ZIMM (maintained by the International GNSS Service (IGS) and available at http://igscb.jpl.nasa.gov) indicates several receiver, firmware, and antenna changes over the duration of the time series. Estimation of offsets using short

(2 year) segments of data centered on the change indicated no significant ($>2\sigma$) values, and so no additional offset parameters were included in the model here or below. The 16 year edited time series, along with the final best fit standard model, are shown in Figure 3b.

[20] The PSD for the 16 year edited time series of Figure 3b is shown by the black curve in Figure 4. This PSD has a number of features of interest to this study. For $f > 1$ cpy the spectrum is roughly that of an inverse power law with $\alpha = 0.9$. (For visual comparison, the gray curve is equation (15) with $C_a^2 + C_b^2 = 2$ mm^2 cpy^{-1}, $\alpha = 0.9$, and $f_\circ = 1$ cpy.) Spectral peaks are obvious near 1 cpy and 4 cpy, although there is significant power distributed broadly between 2 and 3 cpy. The peak near 1 cpy occurs at 0.98 cpy. Given the frequency resolution (∼0.06 cpy) this peak could be at either the climatic or draconitic annual frequency. The peak near 1 cpy is broad and strong, and the total variance within this peak (0.6 cpy $\leq f \leq$ 1.4 cpy) is 21.3 mm^2. This peak appears to have too much power to be associated with errors that manifest themselves at the draconitic annual period [e.g., *Tregoning and Watson*, 2009; *King and Watson*, 2010], and so is likely dominated by climatic seasonal variations. The peak near 4 cpy occurs at 4.19 cpy, close to the draconitic harmonic of 4.16, so power at this frequency may be associated with errors that manifest themselves within the draconitic spectrum. For $f < 1$ cpy, there is a hint that the power spectrum flattens out relative to the f^{-1} behavior for higher frequencies.

[21] To illustrate the stochastic variability of the seasonal signal in this time series, we band-pass filter the edited data, allowing frequencies between 0.7 cpy and 2.5 cpy to pass. (To deal with data gaps, we first interpolate the data set to create a daily sampled time series.) The band-pass-filtered data are shown in Figure 3c. The seasonal signal and its variability are clearly visible in Figure 3c. The seasonal amplitudes reach a maximum of 7–10 mm during 2003–2005 and a minimum of 2–4 mm between 2007 and 2009. Figure 3d shows the residuals of the edited time series to the standard model, band-pass filtered as per Figure 3c. The residuals are, of course, smaller in amplitude than the original data, but the seasonal signature is still clear. It has been more homogenized, and the semiannual variations are more evident, especially in the earlier part of the time series.

[22] The red curve in Figure 4 is the PSD for the residuals to the standard seasonal model shown in Figure 3b. This PSD still shows a significant amount of power near the annual frequency. The peak has shifted somewhat to 1.07 cpy, which may indicate that there is some power at the draconitic annual frequency, but it is not possible to conclusively determine this due to the frequency resolution of the PSD. However, the breadth of the peak still indicates that the periodic signal is time-variable. The residual power near the annual frequency is consistent with the band-passed residuals of Figure 3c, which still show a strong seasonal variability.

[23] We have analyzed these time series with a linear Kalman filter, described below, that allows for random walk variation in the rate and sinusoidal amplitudes [*Murray and Segall*, 2005; *Wernicke and Davis*, 2010]. In the stochastic filter, we used variance rate values of 1 mm^2 yr^{-3} for the rate term and 0.5 mm^2 yr^{-1} for the sinusoidal amplitudes. The estimated model for the edited time series is shown in red in
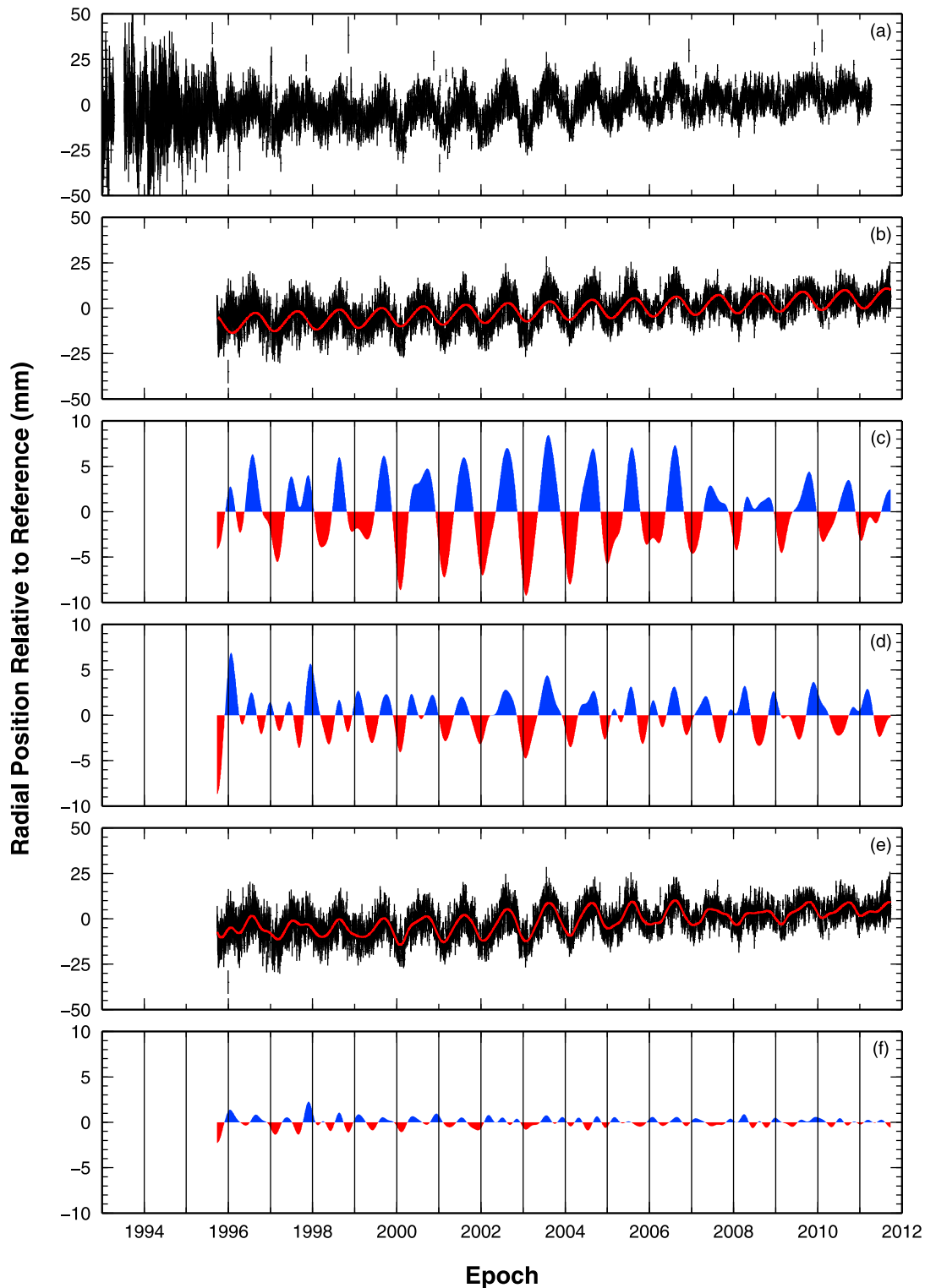
Figure 3. Various treatments of estimates of the vertical coordinate, relative to a reference position, for the GNSS site ZIMM, illustrating the effect of variable seasonal amplitudes. (a) Original time series (plus 1σ error bars) from SOPAC. (b) Edited (see text) 16 year time series (black), along with the "standard model" (red) consisting of the best fit straight line plus annual and semiannual sinusoids. (c) Time series after band-pass filtering to allow frequencies of 0.7–2.5 cpy to pass (see text), with areas under the positive values in blue and areas under the negative values in red. Vertical grid lines are spaced by 1 year. (d) Band-pass-filtered residuals to the "standard model." (e) Edited 16 year time series (black) along with a best fit stochastic seasonal model (red). (f) Band-pass-filtered residuals to the stochastic filter model. Notice the scale differences for Figures 3c, 3d, and 3f).
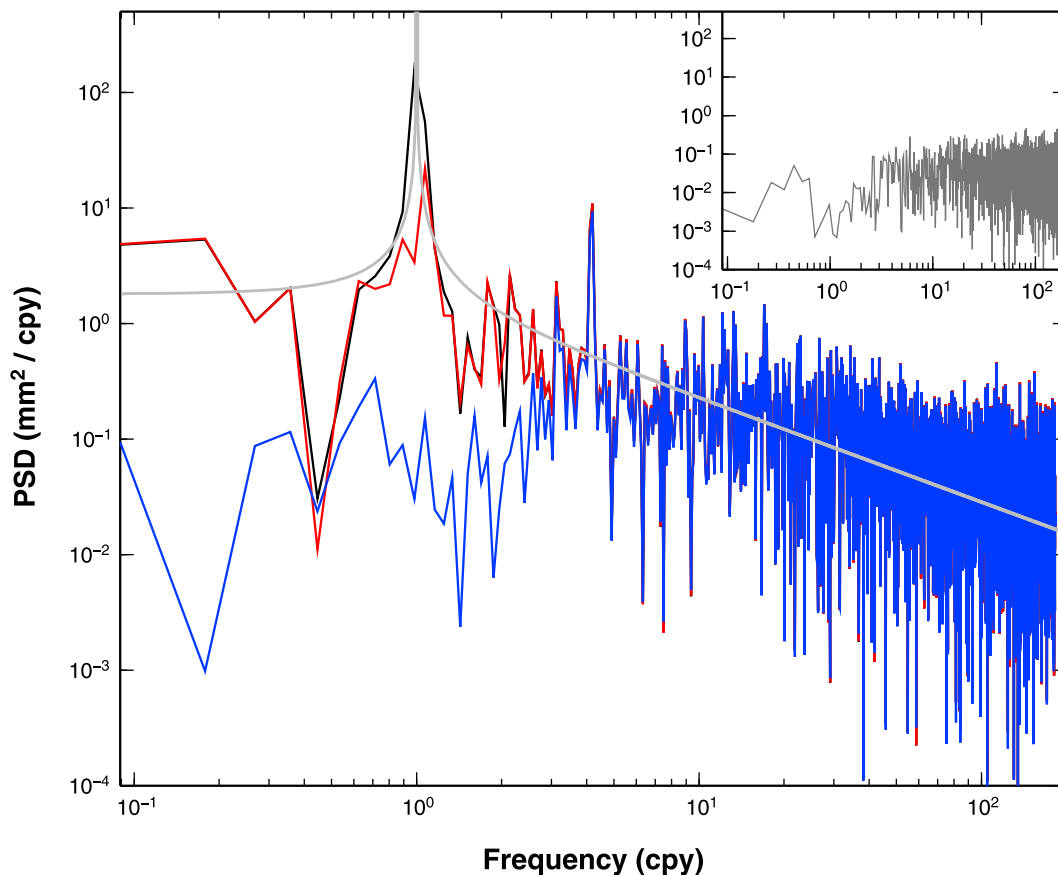
Figure 4. PSDs for several of the ZIMM time series of Figure 3. Black curve is the PSD of the 16 year edited time series (Figure 3b). Red curve is the PSD of the residuals to the standard seasonal model (difference between black and red curves in Figure 3b). Blue curve is the PSD of residuals to the Kalman-filtered model (difference between black and red curves in Figure 3e). The PSDs were calculated using a fast Fourier transform approach and a Welch window [*Press et al.*, 2002]. The light gray curve is equation (15) with $C_a^2 + C_b^2 = 2$ mm^2 cpy^{-1}, $\alpha = 0.9$, and $f_\circ = 1$ cpy. The inset shows residuals (dark gray) to a Kalman-filtered sequence of random zero-mean white noise values having the standard deviations of the original data. This particular Kalman filter, described in the text, suppresses frequencies in the seasonal band and lower.

Figure 3e. Comparison of the red curves in Figures 3b and 3e demonstrates that a stochastic seasonal process is justified. The band-passed residuals to the Kalman filter model (Figure 3f) contain very little seasonal signal. This observation is reflected in the PSD of the Kalman filter residuals (blue curve in Figure 4), which has significantly reduced power (~30 dB) with no obvious peaks in the band-pass region.

[24] The Kalman-filtered residuals maintain power near 4 cpy, indicating that the response of the Kalman filter across the band is not constant. The dark gray curve in the inset in Figure 4 shows the residuals of a Kalman-filtered zero-mean white noise sequence in which the standard deviation of each point is the same as that of the original time series. The filter passes most frequencies except in the seasonal band and below. This frequency response is a result of the Kalman filter's balancing of the noise process (as indicated by the model and the variances input to the filter) and the data uncertainties. As seen in Figure 3e, the Kalman filter solution is quite smooth and, by nature of this

balancing, cannot reflect high-frequency variability unless the data uncertainties were much smaller.

[25] We implemented a simplified model for equations (10)–(12) in the Kalman filter, based on the assumption that the dynamic models for δa_1 and δb are the same:

$$x(t) = a'(t)\cos 2\pi f_\circ t + b'(t)\sin 2\pi f_\circ t. \tag{17}$$

We model $a'(t)$ and $b'(t)$ as random walk processes. The full model implemented in the stochastic filter used for Figure 3 and below includes both annual and semiannual terms:

$$\begin{aligned}
x(t) = x_\circ &+ v(t)(t - t_\circ) \\
&+ a_1'(t)\cos 2\pi f_\circ(t - t_\circ) + b_1'(t)\sin 2\pi f_\circ(t - t_\circ) \\
&+ a_2'(t)\cos 4\pi f_\circ(t - t_\circ) + b_2'(t)\sin 4\pi f_\circ(t - t_\circ),
\end{aligned} \tag{18}$$

where $v(t)$, $a_1'(t)$, $b_1'(t)$, $a_2'(t)$, and $b_2'(t)$ are modeled as random walk parameters and $t_\circ$ is a reference epoch. The difference in how the seasonal components of equations (18) and (12) are modeled lies in the fact that in equation (12) the stochastic amplitudes $\delta a_1(t)$ and $\delta b(t)$ could be statistically independent

(although we have not needed to make use of this property), whereas we know that $a'_k(t)$ and $b'_k(t)$ are probably not. This correlation, if we knew its value, could be included in the dynamic model for the amplitude parameters (by having the noise covariance matrix have nondiagonal elements). Since we do not know this correlation, our dynamic model does not include it. It will be clear from the solutions that we perform below, however, that the data naturally constrain the parameters to have nearly constant phase.

[26] Time series of surface mass variations from glaciated regions can have large seasonal signals, as well as large rates and significant variations in all these parameters. Figures 5a–5c show time series of surface mass in terms of equivalent water depth [e.g., *Wahr et al.*, 1998] integrated for the region of Alaskan glaciers [*Tamisiea et al.*, 2005], calculated from Gravity Recovery and Climate Experiment (GRACE) satellite data. No scaling has been performed to correct for the undersampling of ice sheet mass changes by areal integration [*Tamisiea et al.*, 2005], nor have the effects of contamination been carefully removed, since we are using these estimates only to illustrate the impact of rate variability and stochastic seasonal processes. Visual inspection of the time series of mass change (black circles in Figures 5a (top) to 5c (top)) indicate that both the seasonal amplitudes and the rate have changes over the ~9 year time span since the beginning of GRACE data acquisition, although it can be difficult to separate these variations. The best fit standard model, shown in red in Figure 5a (top), does not capture these variations well, as demonstrated in the bottom plot of this frame in which the postfit residuals are shown. The WRMS residual for this model is 26 mm, and large systematic variations are evident, both at time scales of the entire time series and at 1–2 year time scales. Because the amplitude and rate parameters were not allowed to vary in the standard model, we represent them in Figure 5d as time series with constant values. (The error bars are almost too small to be observed in Figure 5d.)

[27] In Figure 5b we show the same time series of mass changes, but the model represents a best fit model in which the rate is allowed to vary stochastically but the seasonal amplitudes remain constant. (We call this model the "variable rate" solution for brevity.) The residuals in this frame have much less systematic "long-term" behavior, but the shorter term variability still remains. (The WRMS residual for this model is 17 mm.) The estimated rate parameter (Figure 5e, top) displays some variability during 2004–2006, during which period the residuals are large. The estimated rate of mass change is actually positive (at the ~2σ level) in 2008.

[28] The results for the full stochastic model, including variable rate and a stochastic seasonal model, indicate a much better fit (Figure 5c), with a WRMS residual of 7 mm and little systematic nature, except for the period of 2009–2011. The estimated rate parameter for the full stochastic model (Figure 5f, top) is smoother than that of the variable rate model in the 2005–2006 time period. It seems likely that the rate parameter in the variable rate solution absorbed some of the seasonal variability. Formally, the parameter estimates from the full stochastic solution are more uncertain than those of the stochastic rate-only because the number of degrees of freedom for the full stochastic solution is less than that for the rate-only solution; in the absence of systematic error, the parameter estimates from the full stochastic solution should therefore be noisier, not smoother.

[29] The value for the estimated annual amplitude (Figure 5f, bottom, blue points) increases to a maximum and then subsides during 2005–2006. The rate parameter for the full stochastic model does not become significantly positive in 2008 (i.e., within error they may be negative, in contrast to the variable rate solution), and becomes less positive in 2011, indicating that the positive rate result at these times for the variable rate solution may also be influenced by use of the stochastic seasonal model.

[30] The phase offset estimates for the stochastic model (Figure 5f, bottom, red points) indicate that, as we assumed, the phase offset does not vary greatly (less than $\pm 15°$) with time. There seems to be a slight negative correlation between the phase and amplitude during the period 2008–2010. However, this is a period of rapid amplitude variability that is not completely captured by the filter using the variance rates we have chosen for the stochastic model. We used a value of 1000 mm^2 yr^{-3} for the rate parameter and for all the seasonal amplitudes (annual and semiannual) we used 500 mm^2 yr^{-1}. The postfit residuals (Figure 5c, bottom) also show some systematic variability during this time period, and the correlation between amplitude and phase may be an artifact of the inadequate fit. (This inadequacy may indicate that larger variance parameters are required or that the Kalman-smoothed random walk model does not allow rapid enough variability. Since this analysis is being performed only to provide an example of a treatment with variable amplitude parameters and not to explore the statistics of melting glaciers, we do not investigate this issue further.)

5. Discussion and Conclusions

[31] In section 3 we obtained the result that, for frequencies greater than the seasonal signals (say 2.5 cpy), the PSD of a stochastic seasonal process is the PSD of the seasonal amplitudes. Environmental noise is typically red, and often can be expressed in terms of an inverse power law of frequency [e.g., *Vasseur and Yodzis*, 2004]. Therefore, based on the results presented here we might expect that stochastic seasonal variability may contribute to the power spectrum of geodetic time series, since we have demonstrated that removal of annual (plus semiannual, etc.) sinusoids of constant amplitude leaves behind a strong stochastic seasonal component. *Bennett* [2008] also arrived at this conclusion.

[32] For time series estimated from GNSS data, estimation of a constant seasonal amplitude (our "standard model") is usually performed. A number of studies using GNSS time series have confirmed that they have a red PSD, although there has been an active discussion in the literature regarding whether these PSDs are best represented by flicker noise (f^{-1}), random walk (f^{-2}), or even an FOGM process (see equation (16)). One might inquire in light of our results whether some of the observed power in GNSS time series is due to the variable amplitude seasonal signal being modeled using constant amplitude sinusoids. In fact, the FOGM process PSD was considered because the observed power spectra tend to flatten at lowest frequencies [*Langbein and Johnson*, 1997]. This flattening could be a result of removing a trend (thereby decreasing power at the lowest frequencies), or it could also be indicative of a stochastic seasonal process.
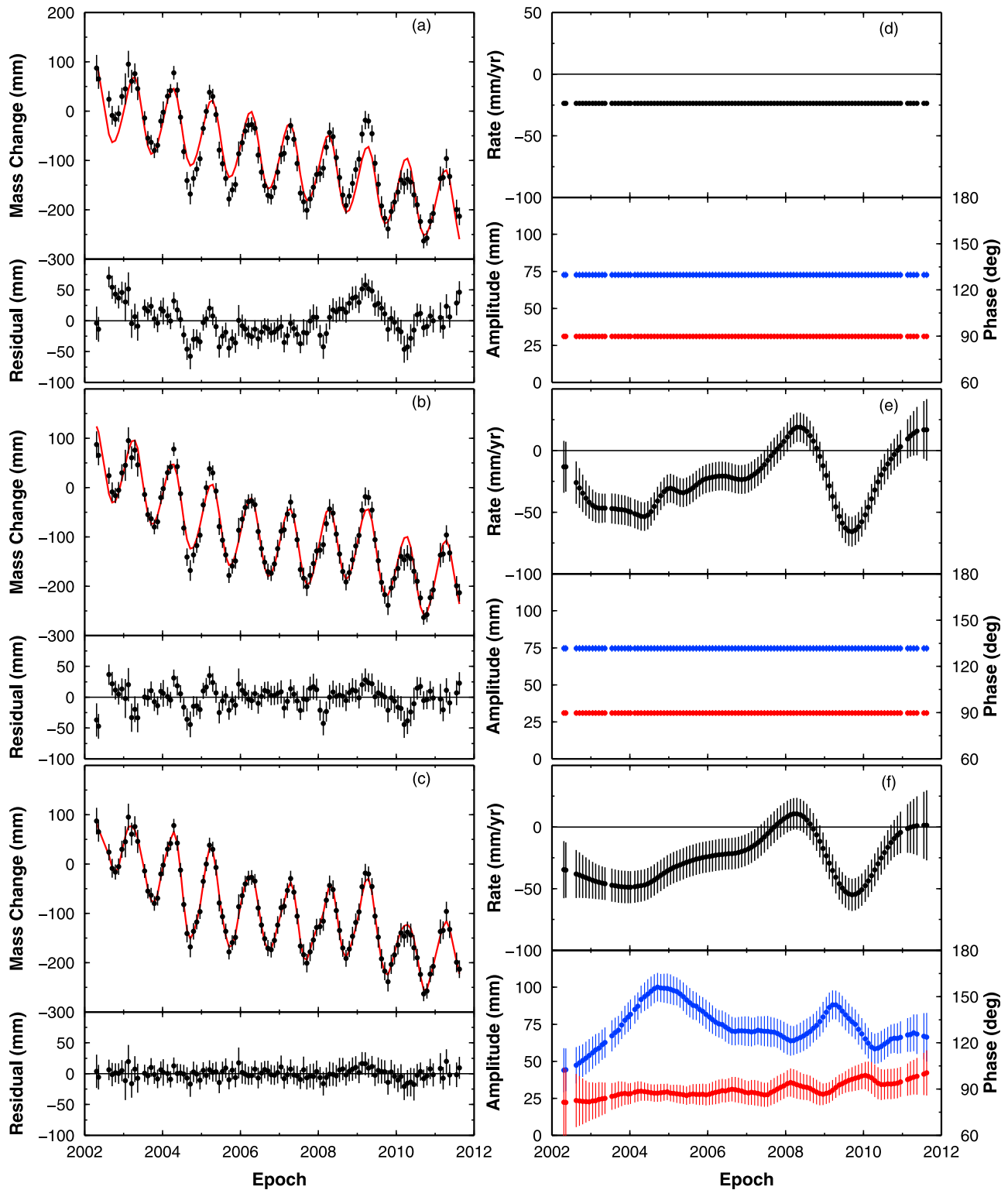
Figure 5. (a–c) Estimates of unscaled mass changes (in terms of equivalent water depth) for Alaska from the GRACE satellite (black) along with the best fit model (red). The residuals are shown beneath each data/model plot. (d–f) The estimated rates (top), annual amplitudes (bottom, blue, left scale) and phase offset (bottom, red, right scale) for each model are shown. Figures 5a and 5d show the standard model. Figures 5b and 5e show the stochastic model that allows only for velocity variations. Figures 5c and 5f show the full stochastic model (rate variations plus stochastic seasonal process). Error bars are 1σ.
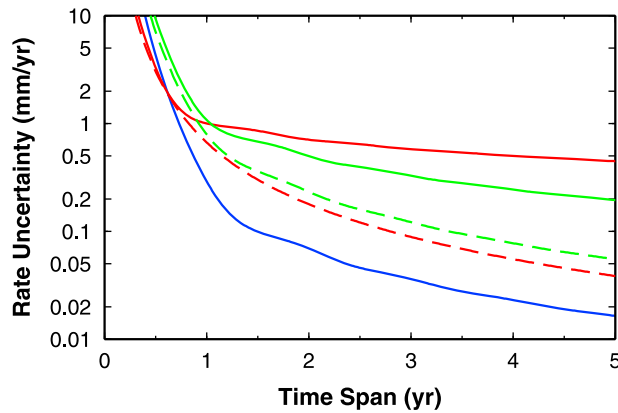
Figure 6. Estimated velocity uncertainty as a function of time series length for a white noise process (blue), a random walk process (red), a stochastic seasonal process with random walk amplitudes (dashed red), a flicker noise process (green), and a stochastic seasonal process with flicker noise amplitudes (dashed green).

[33] *Langbein* [2004] performed a comprehensive analysis of noise in two-color electronic distance meter (EDM) measurements at various sites in California. The measurement time series were analyzed with a model in which changes in rate were allowed but the seasonal amplitudes were constant in time. This study found that the noise for various sites could be best characterized as random walk (for 30% of the data), inverse power law with a spectral index between 1 and 2 (30%), combined band-pass-filtered plus random walk (30%), and combination of band-pass-filtered plus power law (10%). The band-passed-filtered spectrum used by *Langbein* [2004] passed frequencies around 1 cpy, and the success of this model could be indicative of a stochastic seasonal process. Visual inspection of the *Langbein* [2004] time series, especially those from Parkfield [*Langbein* 2004, Figure 5], indicates the presence of a highly variable seasonal signal in several of the time series.

[34] Accounting for a stochastic seasonal process has a significant impact on the estimation of the rate. We found trade-offs between the variable seasonal and rate terms, in agreement with the findings of *Bennett* [2008]. Figure 6 shows the results of simulations for five different time series noise processes: white noise, random walk, flicker noise, seasonal random walk (that is, stochastic seasonal process with random walk amplitudes), and seasonal flicker noise (stochastic seasonal process with flicker noise amplitudes). The covariance matrices for the simulations were set up using the results from *Zhang et al.* [1997] and *Williams* [2003], modified for a seasonal stochastic process. For each process, a constant rate was estimated, as well as seasonal terms that consisted of annual and semiannual sines and cosines. The time series are sampled daily with constant standard deviation of 1.5 mm. The variance of each stochastic process has a value of unity (with various units). In Figure 6 we plot the resulting rate uncertainties as a function of time series length. Comparing the white noise (blue) with random walk (red) and flicker noise (green) curves gives the well-known result [e.g., *Langbein and Johnson*, 1997] that for those colored noise processes the rate uncertainty is much larger, and the decrease with time is much flatter, for the inverse power law cases than for the white noise case. The rate uncertainties for the stochastic seasonal processes (dashed red and green curves in Figure 6) also decrease less rapidly than the white noise case, but these curves parallel that of the white noise curve for times greater than about 2 years. The stochastic seasonal curves (dashed curves) are less than their nonseasonal counterparts (solid curves) due in part to the negative values introduced into a covariance matrix that is otherwise all positive. Looking at it from the point of view of the PSD, the resonances that were formerly at $f = 0$ have been shifted to $f = 1$ cpy. To the extent that this result applies generally to inverse power law processes, noise analyses that do not allow for stochastic seasonal processes run the risk of absorbing some of the seasonal power into the estimates of the nonseasonal noise, thereby significantly overestimating the rate uncertainties.

[35] From our study, we conclude that a stochastic seasonal process should be a standard component in the models for geodetic time series. In this study, we used a Kalman filter to model these variations as random walks [e.g., *Murray and Segall*, 2005; *Wernicke and Davis*, 2010], because is was straightforward to implement, although other approaches have been used [e.g., *Davis et al.*, 2006; *Bennett*, 2008]. Ignoring these variations, however, will contribute to positive correlations in the time series and a reddened power spectrum. The importance of a stochastic seasonal process will, of course, be dependent on the site and the type of time series being considered. In our example that used GRACE mass estimates for Alaska, the seasonal signature practically overwhelms the rate and the changes in both of these parameters can easily be confused. This problem is potentially more complex to solve since both the change in the rate of mass loss and its seasonal variability may truly be correlated because they both are measures of the response of the Alaskan glaciers to climate.

[36] For geodetic position time series (as from GNSS), as the models and techniques used in our data analysis improve, the accuracy of our position estimates improve. There will therefore be more interest in detecting changes in site velocities. In such studies, it is imperative that other known sources of temporal variation such as the variable seasonal signal be modeled [e.g., *Murray and Segall*, 2005; *Davis et al.*, 2006; *Wernicke et al.*, 2008; *Bennett*, 2008; *Wernicke and Davis*, 2010].

[37] Studies of noise in geodetic time series should allow for the presence of a stochastic seasonal process. If the underlying environmental/seasonal noise is an inverse power law, then we find that this will introduce an inverse power law component to the power of the geodetic time series for high frequency ($f \gg f_\circ$), a broad resonance at $f_\circ$, and a flat power for small f. If there are components at harmonics of the annual period (semiannual, for example), the signals will be superimposed.

References

Barrett, P. (2008), The relative contribution of the annual and draconitic periods in GPS station position spectra, paper presented at the 2008 IGS Workshop, Natl. Geod. Surv., Miami Beach, Fla., 2–6 June.

Beavan, J. (2005), Noise properties of continuous GPS data from concrete pillar geodetic monuments in New Zealand and comparison with data from U.S. deep drilled braced monuments, *J. Geophys. Res.*, *110*, B08410, doi:10.1029/2005JB003642.

Bell, J., F. Amelung, A. Ramelli, and G. Blewitt (2002), Land subsidence in Las Vegas, Nevada, 1935–2000: New geodetic data show evolution, revised spatial patterns, and reduced rates, *Environ. Eng. Geosci.*, *8*(3), 155–174, doi:10.2113/8.3.155.

Bennett, R. A. (2008), Instantaneous deformation from continuous GPS: Contributions from quasi-periodic loads, *Geophys. J. Int.*, *174*, 1052–1064, doi:10.1111/j.1365-246X.2008.03846.x.

Blewitt, G., and D. Lavallée (2002), Effect of annual signals on geodetic velocity, *J. Geophys. Res.*, *107*(B7), 2145, doi:10.1029/2001JB000570.

Bos, M., L. Bastos, and R. M. S. Fernandes (2010), The influence of seasonal signals on the estimation of the tectonic motion in short continuous GPS time-series, *J. Geodyn.*, *49*, 205–209, doi:10.1016/j.jog.2009.10.005.

Bracewell, R. N. (1978), *The Fourier Transform and Its Applications*, 444 pp., McGraw-Hill, New York.

Davis, J. L., T. A. Herring, I. I. Shapiro, A. E. E. Rogers, and G. Elgered (1985), Geodesy by radio interferometry: Effects of atmospheric modeling errors on estimates of baseline length, *Radio Sci.*, *20*, 1593–1607, doi:10.1029/RS020i006p01593.

Davis, J. L., B. P. Wernicke, S. Bisnath, N. A. Niemi, and P. Elósegui (2006), Subcontinental-scale crustal velocity changes along the Pacific-North American plate boundary, *Nature*, *441*(7097), 1131–1134, doi:10.1038/nature04781.

Durbin, J., and S. J. Koopman (2001), *Time Series Analysis by State Space Methods*, Oxford Univ. Press, New York.

Elósegui, P., J. L. Davis, R. T. K. Jaldehag, J. M. Johansson, A. E. Niell, and I. I. Shapiro (1995), Geodesy using the Global Positioning System: The effects of signal scattering on estimates of site position, *J. Geophys. Res.*, *100*(B7), 9921–9934, doi:10.1029/95JB00868.

Halley, J. M., and P. Inchausti (2004), The increasing importance of 1/*f*-noises as models of ecological variability, *Fluct. Noise Lett.*, *4*(2), R1–R26, doi:10.1142/S0219477504001884.

Herring, T. A. (1986), Precision of vertical position estimates from very long baseline interferometry, *J. Geophys. Res.*, *91*, 9177–9182, doi:10.1029/JB091iB09p09177.

King, M. A., and C. S. Watson (2010), Long GPS coordinate time series: Multipath and geometry effects, *J. Geophys. Res.*, *115*, B04403, doi:10.1029/2009JB006543.

King, M. A., C. S. Watson, N. T. Penna, and P. J. Clarke (2008), Subdaily signals in GPS observations and their effect at semiannual and annual periods, *Geophys. Res. Lett.*, *35*, L03302, doi:10.1029/2007GL032252.

King, N. E., et al. (2007), Space geodetic observation of expansion of the San Gabriel Valley, California, aquifer system, during heavy rainfall in winter 2004–2005, *J. Geophys. Res.*, *112*, B03409, doi:10.1029/2006JB004448.

Langbein, J. (2004), Noise in two-color electronic distance meter measurements revisited, *J. Geophys. Res.*, *109*, B04406, doi:10.1029/2003JB002819.

Langbein, J. (2008), Noise in GPS displacement measurements from southern California and southern Nevada, *J. Geophys. Res.*, *113*, B05405, doi:10.1029/2007JB005247.

Langbein, J., and H. Johnson (1997), Correlated errors in geodetic time series: Implications for time-dependent deformation, *J. Geophys. Res.*, *102*, 591–603, doi:10.1029/96JB02945.

Murray, J. R., and P. Segall (2005), Spatiotemporal evolution of a transient slip event on the San Andreas fault near Parkfield, California, *J. Geophys. Res.*, *110*, B09407, doi:10.1029/2005JB003651.

Park, K.-D., R. S. Nerem, M. S. Schenewerk, and J. L. Davis (2004), Site-specific multipath characteristics of global IGS and CORS GPS sites, *J. Geod.*, *77*, 799–803, doi:10.1007/s00190-003-0359-9.

Penna, N. T., and M. P. Stewart (2003), Aliased tidal signatures in continuous GPS height time series, *Geophys. Res. Lett.*, *30*(23), 2184, doi:10.1029/2003GL018828.

Penna, N. T., M. A. King, and M. P. Stewart (2007), GPS height time series: Short-period origins of spurious long-period signals, *J. Geophys. Res.*, *112*, B02402, doi:10.1029/2005JB004047.

Prawirodirdjo, L., Y. Ben-Zion, and Y. Bock (2006), Observation and modeling of thermoelastic strain in Southern California Integrated GPS Network daily position time series, *J. Geophys. Res.*, *111*, B02408, doi:10.1029/2005JB003716.

Press, W. H., S. A. Teukolsky, W. T. Vetterling, and B. P. Flannery (2002), *Numerical Recipes in C*, 2nd ed., Cambridge Univ. Press, New York.

Ray, J., Z. Altamimi, X. Collilieux, and T. van Dam (2008), Anomalous harmonics in the spectra of GPS position estimates, *GPS Solut.*, *12*, 55–64, doi:10.1007/s10291-007-0067-7.

Santamaría-Gómez, A., M.-N. Bouin, X. Collilieux, and G. Wöppelmann (2011), Correlated errors in GPS position time series: Implications for velocity estimates, *J. Geophys. Res.*, *116*, B01405, doi:10.1029/2010JB007701.

Tamisiea, M. E., E. Leuliette, J. L. Davis, and J. X. Mitrovica (2005), Constraining hydrological and cryospheric mass flux in southeastern Alaska using space-based gravity measurements, *Geophys. Res. Lett.*, *32*, L20501, doi:10.1029/2005GL023961.

Tregoning, P., and C. Watson (2009), Atmospheric effects and spurious signals in GPS analyses, *J. Geophys. Res.*, *114*, B09403, doi:10.1029/2009JB006344.

van Dam, T., J. Wahr, P. C. D. Milly, A. B. Shmakin, G. Blewitt, D. Lavallée, and K. M. Larson (2001), Crustal displacements due to continental water loading, *Geophys. Res. Lett.*, *28*, 651–654, doi:10.1029/2000GL012120.

Vasseur, D. A., and P. Yodzis (2004), The color of environmental noise, *Ecology*, *85*(4), 1146–1152, doi:10.1890/02-3122.

Wahr, J., M. Molenaar, and F. Bryan (1998), Time variability of the Earth's gravity field: Hydrological and oceanic effects and their possible detection using GRACE, *J. Geophys. Res.*, *103*, 30,205–30,229, doi:10.1029/98JB02844.

Wernicke, B., and J. L. Davis (2010), Detecting large scale intracontinental slow-slip events (SSEs) using geodograms, *Seismol. Res. Lett.*, *81*, 694–698, doi:10.1785/gssrl.81.5.694.

Wernicke, B., J. L. Davis, N. A. Niemi, P. Luffi, and S. Bisnath (2008), Active megadetachment beneath the western United States, *J. Geophys. Res.*, *113*, B11409, doi:10.1029/2007JB005375.

Wessel, P., and W. H. F. Smith (1998), New, improved version of generic mapping tools released, *Eos Trans. AGU*, *79*(47), 579.

Williams, S. D. P. (2003), The effect of coloured noise on the uncertainties of rates estimated from geodetic time series, *J. Geod.*, *76*, 483–494, doi:10.1007/s00190-002-0283-4.

Williams, S. D. P., Y. Bock, P. Fang, P. Jamason, R. M. Nikolaidis, L. Prawirodirdjo, M. Miller, and D. Johnson (2004), Error analysis of continuous GPS position time series, *J. Geophys. Res.*, *109*, B03412, doi:10.1029/2003JB002741.

Young, P. C., C. N. Ng, K. Lane, and D. Parke (1991), Recursive forecasting, smoothing and seasonal adjustment of non-stationary environmental data, *J. Forecast.*, *10*, 57–89, doi:10.1002/for.3980100105.

Zhang, J., Y. Bock, H. Johnson, P. Fang, S. Williams, J. Genrich, S. Wdowinski, and J. Behr (1997), Southern California Permanent GPS Geodetic Array: Error analysis of daily position estimates and site velocities, *J. Geophys. Res.*, *102*(B8), 18,035–18,055, doi:10.1029/97JB01380.

J. L. Davis, Lamont-Doherty Earth Observatory, Columbia University, 61 Route 9W, Palisades, NY 10964, USA. (jdavis@ldeo.columbia.edu)

M. E. Tamisiea, National Oceanography Centre, Joseph Proudman Building, 6 Brownlow St., Liverpool L3 5DA, UK. (mtam@noc.ac.uk)

B. P. Wernicke, Division of Geological and Planetary Sciences, California Institute of Technology, 1200 E. California Blvd., Mail Stop 100-23, Pasadena, CA 91125, USA. (brian@gps.caltech.edu)